FEATURE ARTICLE

Toward Level-to-Level Energy Transfers in Photosynthesis: The Fenna−Matthews−Olson Protein

Sergei Savikhin, Daniel R. Buck, and Walter S. Struve*

Ames Laboratory—USDOE and Department of Chemistry, Iowa State University, Ames, Iowa 50011

Received: February 17, 1998; In Final Form: May 5, 1998

The trimeric Fenna−Matthews−Olson (FMO) protein is a bacteriochlorophyll (BChl) *a* antenna complex, whose X-ray structure is now known at the atomic level for two green sulfur bacterial species (*Prosthecochloris aestuarii* and *Chlorobium tepidum*). Its steady-state Q_y absorption spectrum at low temperature exhibits considerable structure, with at least eight bands attributable to well-defined (groups of) BChl *a* exciton levels. The low-temperature absorption difference spectra of *Cb. tepidum* trimers excited at 789 nm are correspondingly multifeatured, and they show rich spectral evolution due to femtosecond and picosecond electronic energy transfers. Global analyses of these time-dependent ΔA spectra lead to a phenomenological scenario for cascading and branching among exciton level groups responsible for specific steady-state absorption bands. The missing link in our understanding of structure−function causality in this protein stems from a lack of an ab initio theory for the effects of known protein environments on BChl *a* transition energies; this problem still limits our insights into the workings of spectrally heterogeneous antennas with multiple nonequivalent pigment sites. Optical anisotropy studies strongly suggest that FMO excitations are typically localized to the 7 BChl *a* pigments within one protein subunit, rather than delocalized over the whole trimer. This localization occurs because the resonance couplings between BChls belonging to different subunits (<20 cm^{-1}) are several times smaller than the diagonal energy disorder ($\sim$70 cm^{-1}). Strong oscillations appear in the anisotropies ($\sim$220 fs period) for pump−probe wavelengths that simultaneously overlap both of the exciton level groups responsible for the 825 and 815 nm bands in the Q_y spectrum. These are not vibational coherences, but arise from quantum beating between levels with nearly perpendicular transition moments.

Introduction

The Fenna−Matthews−Olson (FMO) complex is a trimeric bacteriochlorophyll (BChl) *a*−protein complex that promotes electronic energy transfers from the light-harvesting antenna to reaction centers in green sulfur bacteria.[1] In these organisms, the primary light-harvesting function is served by the chlorosome, an ellipsoidal body encased in a phospholipid/glycolipid envelope that is appressed to the inner cytoplasmic membrane.[1−3] The chlorosome contains some 10 000 BChl *c*, *d*, and *e* pigments, organized into rodlike aggregates absorbing at $\sim$740 nm. Electronic excitations in the BChl *c/d/e* antenna travel through a crystalline baseplate (believed to consist of FMO complexes, which absorb at $\sim$809 nm at room temperature) prior to being trapped at photochemical reaction centers.[3]

The three-dimensional X-ray structure of FMO trimers from the green bacterium *Prosthecochloris aestuarii* (which predated by several years the much-celebrated structure of the reaction center from the purple bacterium *Rhodopseudomonas viridis*[4]) was the first one revealed with atomic resolution for any photosynthetic pigment−protein complex.[5−7] Olson and Romano[8] showed that a water-soluble BChl *a*−protein complex accounts for $\sim$5% of the bacteriochlorophyll pigments in green sulfur bacteria. This protein was crystallized as hexagonal rods; X-ray structure analysis[7] revealed that it exists as trimers of identical 50 kDa subunits organized about a 3-fold rotation axis (Figure 1). The presence of a C_3 axis is widespread (but not universal) in photosynthetic pigment−protein complexes.[9−12] Each protein subunit in an FMO trimer contains a β-sheet with 16 strands that enfold seven pentacoordinate BChl *a* pigments with positions and orientations that are perfectly repeated (in the crystallographic sense) from one subunit to the next. The Mg atoms of BChls 1, 3, 4, 6, and 7 (Figure 1) are ligated to histidine residues, while that in BChl 5 is coordinated to a leucine side chain. For BChl 2, the fifth ligand is a water molecule. Nearest-neighbor Mg−Mg distances range from 11 to 15 Å; while there are no sandwich-dimer interactions similar to that in the bacterial reaction center special pair, there are close edge-to-edge contacts. The phytyl chains are packed into a hydrophobic core in the central space between BChls. Very recently, Li et al.[13] determined the X-ray structure of FMO trimers from the green sulfur bacterium *Chlorobium tepidum*. The FMO protein sequences for *Pc. aestuarii* and *Cb. tepidum* are 78% homologous, and all pigment-binding residues are conserved.[14,15] The 80 unconserved residues either are on the protein periphery or are interior residues that do not interact directly with pigments. Interestingly, the respective pigment positions/orientations in the two species are nearly superimposable, with essentially the same Mg−Mg distances; the principal species differences lie in the extent of puckering[13] in

S1089-5647(98)01186-9 CCC: $15.00
Published on Web 06/26/1998

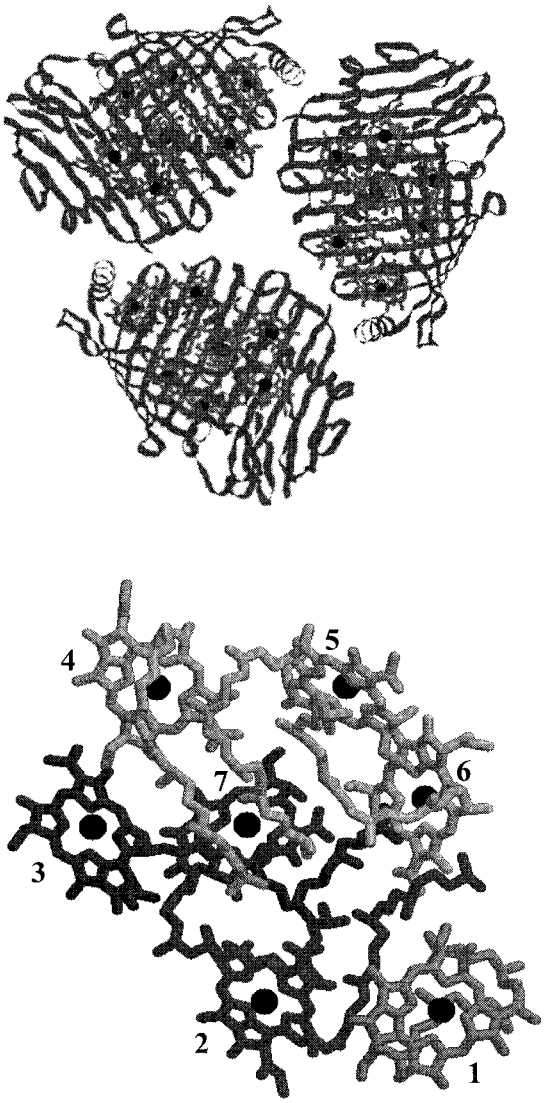

Figure 1. FMO trimer structure from the green bacterium *Pc. aestuarii* (top); arrangement of the seven BChl *a* pigments in one subunit (bottom). Ribbons are strands of protein β-sheets; dark spheres are Mg atoms. (From Protein Data Base coordinates of Tronrud et al.[16])

the BChl macrocycles (more pronounced in *Pc. aestuarii*[16] than in *Cb. tepidum*).

The early discovery of the FMO structure from *Pc. aestuarii* raised hopes that this protein might be pivotal in the revelation of structure−function relationships in photosynthetic antennas. After some 20 years, this scenario has not come to pass. The FMO pigment organization shares more in common with higher green plant antennas (with their close pigment spacings and nonrandom site inhomogeneities) than the LH1/LH2 antennas in purple bacteria[17] or the C-phycocyanin[18] and allophycocyanin antennas from cyanobacteria. Spectroscopic and kinetic studies have nevertheless been considerably more fruitful in the latter systems than in the FMO protein, for two reasons: (a) the room-temperature kinetics of primary energy transfers in the FMO protein extend well into the femtosecond regime, unlike the B800 → B850 energy transfers in LH2[17] and most energy transfers in C-phycocyanin[18] and allophycocyanin; and (b) the BChl pigments in the irregular FMO structure (Figure 1) exhibit a minimum of seven independent site energies for excitation of BChl *a* pigments into their lowest excited singlet (Q_y) state. (There are only two nonequivalent BChl *a* pigment sites in the circular B850 aggregate of the LH2 antennas and only three nonequivalent phycocyanobilin pigments in C-phycocyanin or allophycocyanin.) The first problem has been alleviated by the arrival of stable femtosecond Ti:sapphire lasers in photosynthesis laboratories in the early 1990s. The second problem—and the lack of an ab initio theory for predicting BChl *a* transition energies in different protein sites—still hinders our understanding of excited-state electronic structure and energy-transfer processes in most antennas. This theme permeates current spectroscopic and theoretical discussions of the FMO protein.

FMO Excited States: The Q_y Spectrum

The close BChl pigment separations in the FMO protein give rise to appreciable resonance interactions between the chromophore Q_y states, with the consequence that electronic excitations cannot be regarded as localized on single chromophores. These exciton couplings cause wavelength shifts and redistributions of oscillator strengths in the Q_y electronic absorption spectrum, as well as intense circular dichroism (CD) signals that have no counterpart in the (far weaker) CD spectra of individual pigments in proteins. While the absorption and CD spectra of FMO trimers from *Pc. aestuarii* are essentially featureless (due to inhomogeneous broadening) in solution at room temperature, the 77 K absorption (CD) spectrum reported by Philipson and Sauer[19] (hereafter PS) reveals at least five bands, at 792 (787) nm, 804 (800) nm, 813 (812) nm, 817 (814) nm, and 824 (823) nm. Olson, Ke, and Thompson[20] (hereafter OKT) later reported absorption and CD spectra of similar FMO trimers at 77 K. While the OKT absorption spectrum qualitatively resembles the PS spectrum, the CD spectra are significantly different. The longest-wavelength absorption bands (near 805, 815, and 825 nm) appear at similar positions for FMO trimers from *Pc. aestuarii* and *Cb. tepidum*, but with different dipole strengths: the respective bands exhibit relative absorbances of 0.79:1.00:0.33 in *Pc. aestuarii*[20] and 1.07:1.00:0.42 in *Cb. tepidum* (cf. Figure 3). A spectral hole-burning study of FMO trimers from *Pc. aestuarii* revealed eight distinct exciton components in the Q_y spectrum.[21] Since each FMO protein subunit only encloses seven BChl pigments, this implied that resonance interactions between BChls belonging to different protein subunits markedly influenced its absorption spectrum. The two lowest components, separated by 40 cm^{-1}, appeared at 824 and 827 nm. The higher components showed hole widths of $\sim$50 cm^{-1}, corresponding to level relaxation times on the order of 100 fs. This lifetime broadening precluded observation of further splittings among the higher exciton components, arising from intersubunit interactions. The inhomogeneous widths of the two lowest exciton components was $\sim$20 cm^{-1}; analogous studies of FMO trimers from *Cb. tepidum*[22] reported $\sim$70 cm^{-1} inhomogenous broadening in its lowest exciton levels. Further evidence for strong exciton couplings in FMO trimers emerges in their triplet−singlet absorption difference spectra.[23] In the absence of exciton couplings, the only absorption band that would be influenced by long-lived triplet-state formation is the one corresponding to the BChl pigment with the lowest site energy. In reality, all of the absorption bands are markedly affected when the triplet state is populated; the empirical T−S difference spectrum is that for the ground-state FMO trimer, minus the absorption spectrum of the remaining (exciton-coupled) 20 BChl pigments.

The publication of the FMO crystal structure from *Pc. aestuarii* soon prompted attempts to simulate the Q_y absorption and CD spectra of the protein trimers in cryogenic solvents. (It is now known that FMO trimers are unassociated in solution,[23,24] despite an early report that they form large aggregates.[25]) To

date, all FMO simulations have proceeded by diagonalizing the total electronic Hamiltonian for *N* BChl pigments,

$$\hat{H} = \sum_{p}^{N} \hat{H}_p + \sum_{p<q}^{N} V_{pq} \tag{1}$$

in the set of basis states

$$|\chi_1^{(1)}\rangle = |1*23...\rangle, \quad |\chi_2^{(1)}\rangle = |12*3...\rangle, \quad |\chi_3^{(1)}\rangle = |123*...\rangle, \ ... \tag{2}$$

describing Q_y excitations localized on BChls 1, 2, 3, etc. The off-diagonal Hamiltonian matrix elements

$$H_{ij} = \langle \chi_i^{(1)} | V_{ij} | \chi_j^{(1)} \rangle \tag{3}$$

are dominated by the resonance dipole−dipole interaction when the pigment separations are large compared to the molecular size and when the basis states $|\chi_i^{(1)}\rangle$ are connected to the ground state by a strongly allowed electric dipole transition.[26] For the nearest-neighbor pigment separations in FMO trimers, higher-multipole interactions are likely to be important. The V_{ij} have been evaluated for *Pc. aestuarii*[27−29] using BChl Q_y transition monopoles q_k centered at the pigment nuclei, derived from semiempirical SCF-MO-PPP calculations.[30,31] In the point monopole approximation, the interactions have been computed by summing Coulomb energies over all pairs of transition charges belonging to respective pigments. In the point dipole approximation, the total transition dipole for each pigment is computed from the point monopoles at locations r_k via $\vec{\mu}_i = \sum q_k \vec{r}_k$, and the interactions are evaluated as dipole−dipole energies. In the extended dipole approximation, the transition dipoles are represented as pairs of transition charges separated by finite distance, and the interaction is developed as the sum of four Coulomb energies for each pigment pair. The qualitative picture that emerges from such calculations[28] is that while interactions among the seven pigments complexed to the same protein subunit are as large as ∼190 cm^{-1}, the largest interaction between pigments belonging to different subunit is an order of magnitude smaller than this (∼20 cm^{-1}). This hierachy between intrasubunit and intersubunit interactions has consequences for the extent of exciton localization in real FMO trimers (see below). However, these V_{ij} are likely in serious need of updating, since the semiempirical SCF calculations assumed that the equilibrium geometry of the BChl pigments is the same as that of tetraphenylporphyrin (a macrocycle very different from BChl *a*). While these calculations predict that the lowest electronic transition moment is aligned essentially along the Q_y direction,[30,31] this has never been confirmed experimentally (e.g., by polarized absorption spectroscopy of mixed crystals). The basis set of eq 2 may be too limited, since the true Q_y exciton levels in FMO trimers may have some intermolecular charge-transfer character. Charge-transfer states appear to be important in the BChl *a* LH1 and LH2 antennas from purple photosynthetic bacteria.[32]

The diagonal Hamiltonian matrix elements—the seven nonequivalent BChl *a* site energies—are not measurable. They are influenced by pigment−protein interactions and by BChl ring conformations,[33] which vary considerably among BChls 1−7 in *Pc. aestuarii*.[16] Pearlstein and co-workers[27−29] therefore optimized the seven diagonal energies in parametric fits of theoretical absorption and CD spectra to the PS[19] and OKT[20] experimental spectra. Early attempts to model the PS absorption and CD spectra simultaneously, assuming Q_y-oriented transition moments and using a basis set limited to the seven BChls within one subunit, were unsuccessful.[27] Following the Johnson and Small hole-burning study (which underscored the importance of intersubunit couplings[21]), Pearlstein[28] and Lu and Pearlstein[29] were able to reproduce many of the details of both the PS and OKT spectra. Since the PS and OKT CD spectra are quite different, the 21-pigment exciton simulations of the PS and OKT spectra give contrasting views of the FMO electronic structure (Figure 2). In the OKT fits, BChl 7 has the lowest diagonal energy; the lowest three exciton levels, which account for the Q_y absorption bands at 824 and 827 nm, are dominated by excitations on BChls 6 and 7 (and on the rotationally equivalent BChls 13, 14 and 20, 21). In the PS fits, excitations of BChls 3, 4 predominate in the lowest three exciton levels. Gülen[34] suggested that since CD rotational strengths are sensitive to minor changes in BChl organization (e.g., arising from differences between solution and crystal environments), linear dichroism (LD) and T−S absorption difference spectra may provide better criteria for guiding exciton simulations. By optimizing her simulations of absorption, LD, and T−S absorption difference spectra[23] of *Pc. aestuarii* trimers, she concluded that BChl 6 has the lowest diagonal energy. Very recently, Louwe et al.[35] have concluded that BChl 3 is the lowest-energy pigment, on the basis of seven-pigment simulations of absorption, LD, T−S absorption difference, and Q_y absorption difference spectra of *Pc. aestuarii* trimers. It is fair to say that the ordering of BChl diagonal energies remains controversial. Spectroscopic studies of mutant FMO proteins lacking specific BChls may be informative. Alden et al.[36] recently modeled the LH2 BChl *a*−protein antenna complex from the purple bacterium *Rps. acidophila*, using semiempirical QCFF/PI calculations that introduce excitonic and charge-transfer interactions at the configurational interaction level (rather than using the more limited basis set in eqs 2). It would clearly be of interest to extend such calculations to the FMO protein.

Finally, the exciton states for FMO trimers in a real low-temperature glass (the most common spectroscopic environment) will typically show large departures from the C_3 symmetry envisaged in the 21-pigment simulations, because the inhomogeneous broadening in the lowest exciton levels (∼20 cm^{-1} in *Pc. aestuarii*, ∼70 cm^{-1} in *Cb. tepidum*) is not negligible compared to the largest exciton coupling (∼20 cm^{-1}) between

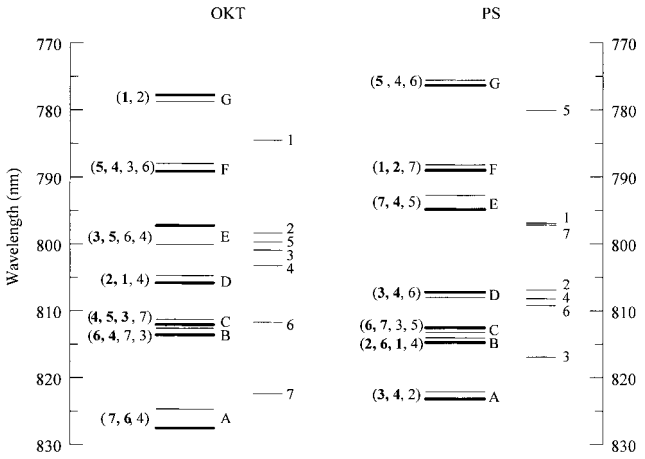

Figure 2. Exciton levels (long bars) and diagonal energies (short bars) from OKT and PS simulations for *Pc. aestuarii* trimers. Exciton level groups are denoted A, B, ..., G in order of energy; thick bars show doubly degenerate levels. Numbers in parentheses give the BChl pigments collectively containing >75% of the excitation density in each level group; boldface numbers show pigments containing >50% of the density. Diagonal energies are labeled with pigment numbers.

BChls belonging to different subunits. Hence, excitation of a Q_y exciton level will produce a statistical distribution of electronic states: few FMO trimers are prepared in 21-pigment states with near-C_3 symmetry. Many more excitations will be essentially localized within a subunit. In this vein, Buck et al.[37] showed that diagonal disorder must be explicitly considered (e.g., by augmenting the BChl diagonal energies with Gaussian noise and averaging the resulting spectra over many trimers) when modeling the Q_y CD spectrum of the FMO protein from *Cb. tepidum*. Excitation localization in FMO trimers similarly has strong leverage on other anisotropic optical properties, such as pump−probe anisotropies (see below). Diagonal energy disorder has considerably less influence on the isotropic absorption spectrum, because the three seven-pigment clusters in an FMO trimer are so weakly coupled.[37]

Excited-State Processes in the FMO Protein

Equilibration among the various exciton components is essentially complete within <1 ps in FMO trimers at room temperature.[38,39] Prior to the arrival of femtosecond Ti:sapphire lasers, kinetic studies of FMO trimers were thus limited to anisotropy decays on the picosecond time scale.[40,41] In one such study, samples of FMO protein from *Pc. aestuarii* were excited between 790 and 825 nm in Tris buffer with 2−3 ps fwhm pulses from a synchronously pumped Styryl 8 dye laser and probed at the same wavelength.[41] The one-color anisotropy

$$r(t) = \frac{\Delta A_{\parallel}(t) - \Delta A_{\perp}(t)}{\Delta A_{\parallel}(t) + 2\Delta A_{\perp}(t)} \qquad (4)$$

was computed from the absorption difference signals $\Delta A_{\parallel}$, $\Delta A_{\perp}$ observed using probe pulses polarized parallel and perpendicular to the pump polarization; it reflects the kinetics of electronic energy transfers between BChl pigments with contrasting orientation. The nominal initial anisotropy $r(0)$ measured at 814 nm was considerably less than 0.4. While this can arise because $r(t)$ has a substantial subpicosecond component buried under the 2−3 ps instrument function, it can also stem from excited-state absorption transitions with polarization different from that of the ground-state → Q_y transitions at the probe wavelength (see below). A single-exponential fit to the subsequent decay in $r(t)$ yielded a 2.3 ps anisotropy decay time. This was assigned to energy transfers between the lowest-energy excitons belonging to different subunits within a trimer, because intrasubunit energy transfers (between nearest-neighbor pigments separated by 11-15 Å) were expected to be considerably faster than ∼2 ps.[26,42] In this scenario, the laser-prepared states equilibrate within <1 ps among the exciton levels within one subunit of a trimer; subsequent energy transfers occur with 6.9 ps kinetics among the lowest-energy exciton components in neighboring subunits. (Energy transfers that occur with rate constant k between rotationally equivalent states in a trimer produce an anisotropy decay with a lifetime of $1/3k$.[43])

Femtosecond pump-probe studies on FMO trimers from *Cb. tepidum* produced a cornucopia of information on the time scales of spectral equilibration between levels at room temperature.[38,39] In an early experiment,[38] trimers excited at 800 nm and probed at 820 nm produced an absorption difference signal, dominated by photobleaching (PB) and stimulated emission (SE) at all times, that exhibited a PB/SE rise time of 370 fs. This yielded a first glimpse at the kinetics of downhill energy transfers between BChl pigments (or exciton states) with SE maxima near 800 and 820 nm. Isotropic two-color experiments using other combinations of pump and probe wavelengths between 798 and 825 nm[39] yielded spectral equilibration kinetics with lifetimes ranging from 55 to 990 fs. This spectral heterogeneity is unsurprising, in view of the FMO proteins's structural irregularity (Figure 1) and the fact that energy-transfer kinetics in an N-pigment system will generally exhibit N distinct lifetimes ($N \geq 7$ in the present case, depending on the extent to which intersubunit transfers contribute during times < 1 ps). An 821 nm one-color anisotropy decay[38] exhibited components with lifetimes 130 fs and 1.7 ps; the latter resembled the 2.3 anisotropy kinetics observed earlier[41] in FMO trimers *from Pc. aestuarii*. One-color experiments at other wavelengths in the Q_y spectrum[39] produced anisotropies with long decay components from 1.4 to 2.0 ps; the latter was observed at 825 nm, where absorption is dominated by the lowest three exciton components.

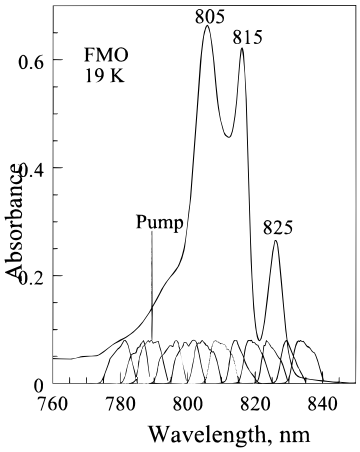

Figure 3. Steady-state absorption spectrum of *Cb. tepidum* trimers at 19 K, with laser excitation and probe spectra superimposed.[44] The excitation spectrum was centered at 789 nm, and probe spectra were spaced by ∼5 nm from 780 to 835 nm.

These experiments reveal little about level-to-level energy-transfer scenarios, because the Q_y absorption spectra of FMO trimers are rendered featureless by inhomogeneous broadening at room temperature. At cryogenic temperatures, absorption bands arising from transitions to specific exciton level groups become well resolved, and group-to-group (if not level-to-level) studies become feasible (Figure 3). Buck et al.[44] obtained two-color ΔA profiles for *Cb. tepidum* trimers pumped at 19 K at 789 nm, which excites one of the highest-lying groups of exciton levels (group F, according to the OKT and PS simulations in Figure 2). Probe wavelengths were spaced at ∼5 nm intervals from 780 to 835 nm, as shown in Figure 3. The probe spectral width was typically 7 nm, and the laser cross-correlation function was ∼250 fs in most cases. Slices of a cubic spline fit to the resulting three-dimensional ΔA versus time and wavelength surface are shown for several time delays from 40 fs to 80 ps in Figure 4. Unlike the room-temperature absorption difference spectra, Figure 4 shows extensive structure and spectral evolution. The 40 fs ΔA spectrum is dominated by an intense PB/SE peak near the excitation wavelength, 789 nm; in addition, it already shows a marked PB/SE feature at ∼805 nm. By 10 ps, this spectrum has essentially equilibrated into one showing a PB/SE maximum near 825 nm. The intervening spectra show PB/SE bands with varying intensities at 790, 805, 815, and 825 nm; these wavelengths are close to the positions of absorption bands in the Q_y steady-state spectrum (Figure 4). A global analysis of the two-color profiles comprising this ΔA surface (using time windows of 8, 80, and 566 ps to help define the long- and short-lifetime components) yields the six lifetimes 170 fs, 630 fs, 2.5 ps, 11 ps, 74 ps, and 840 ps. The decay-

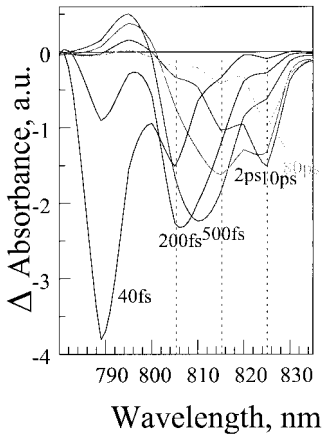

Figure 4. Sections of ΔA versus time and probe wavelength surface[44] at fixed time delays (40 fs to 80 ps), obtained by exciting *Cb. tepidum* trimers with 789 nm pulses at 19 K. Positive and negative signals correspond to ESA and PB/SE, respectively.

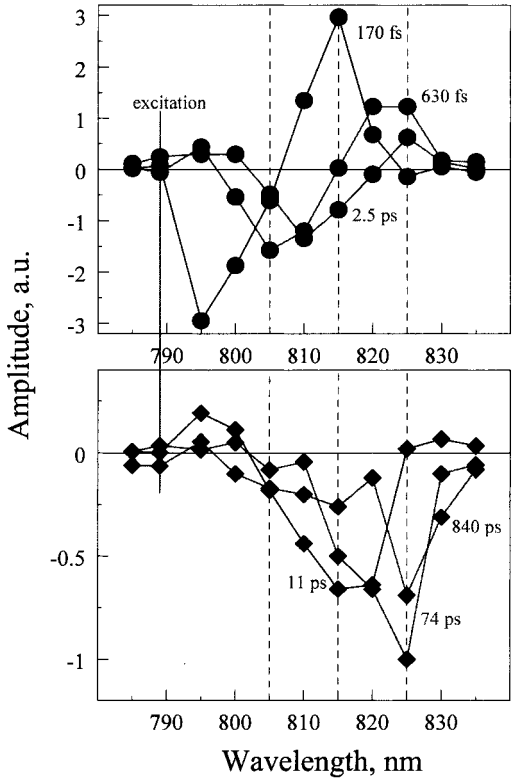

Figure 5. Decay-associated spectra (DAS) from global fits to a set of FMO two-color absorption difference profiles excited at 789 nm (see text). Horizontal coordinate is probe wavelength. Positive and negative DAS amplitudes correspond to SE decay and rise components, respectively.[44]

associated spectra (DAS) for these lifetime components are given in Figure 5. In this figure, positive and negative DAS amplitudes correspond to stimulated emission rise and decay components, respectively. For example, a 170 fs SE decay component for probe wavelengths near 795 nm is coupled with a 170 fs rise component near 815 nm. Similarly, Figure 5 shows 630 fs SE decay and rise components near 805 and 820−825 nm, respectively. If all of the dynamics in the total ΔA signal stemmed from time dependence in SE, the DAS in this figure would suggest the intuitive level relaxation scenario shown in Figure 6. Here, FMO exciton levels that are responsible for SE at 805 nm branch, with 170 and 630 fs kinetics, into groups of levels that are responsible for SE at 815 and 825 nm,

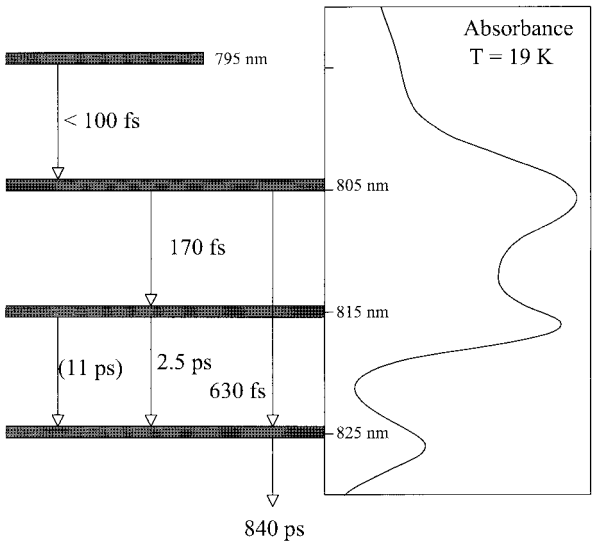

Figure 6. Intuitive relaxation scheme for FMO trimers from *Cb. tepidum* excited at 789 nm at 19 K, derived from global analysis (Figure 5) of time-resolved absorption difference spectra (Figure 4). Exciton level groups are aligned with corresponding absorption bands in the low-temperature steady-state spectrum at right.

respectively. In this sense, the interpretation of the pump−probe DAS in Figure 5 is analogous to that of fluorescence decay-associated spectra, which have been widely used to map electronic energy transfers in spectrally heterogeneous pigment−protein complexes. Parts of this scenario are corroborated by independent two-color experiments excited at 805 nm. An 805 → 815 nm profile (i.e., pumped and probed at 805 and 815 nm, respectively) shows a 140 fs SE rise behavior, which resembles the 170 fs lifetime associated with the corresponding step in the global analysis of Figure 5. Similarly, an 805 → 825 nm experiment yields 600 fs SE rise kinetics, which is similar to the 630 fs global analysis component in Figure 5. The 840 ps component (whose lifetime is not well characterized in the present time windows) likely corresponds to overall BChl *a* Q_y excitation decay. Lifetimes of the same order of magnitude as some of ours were observed by Freiberg et al.[45] in *Cb. tepidum* trimers excited at 800 nm at 15 K. Vulto et al.[46] recently reported time constants of 500 fs, 1.7 ps, 5.5 ps, and 30 ps for interexciton relaxation in *Pc. aestaurii* trimers at 10 K; their kinetic model resembles ours (Figure 6) in that the faster processes occur toward the top of the cascade. Given the reported similarity of the FMO crystal structures for *Pc. aestuarii* and *Cb. tepidum*, it is unclear why the lifetimes appear to be so different between the two species. Part of the variance can arise from differences in experimental conditions. The two species were studied under low[46] and high[44] laser pulse repetition rates, where spurious kinetics can arise from singlet−singlet and singlet−triplet annihilation, respectively. We attempted to minimize the latter in our experiments, where absorbance changes were typically 10^{-5} and sample exposure in our high-speed centrifugal cells[44] was ∼300 pulses; our signals showed no laser power dependence.

In reality, the total ΔA signal has contributions from excited state absorption (ESA) as well as PB and SE. Like SE (and unlike PB[44]), ESA evolves dynamically as relaxation cascades through the various exciton levels. The strongest ESA component arises from electronic transitions between one-exciton levels (whose energies are obtained by diagonalizing the electronic Hamiltonian in the singly excited basis of eq 2) and the two-exciton levels, whose energies lie at approximately twice those of the one-exciton levels. The two-exciton states can be

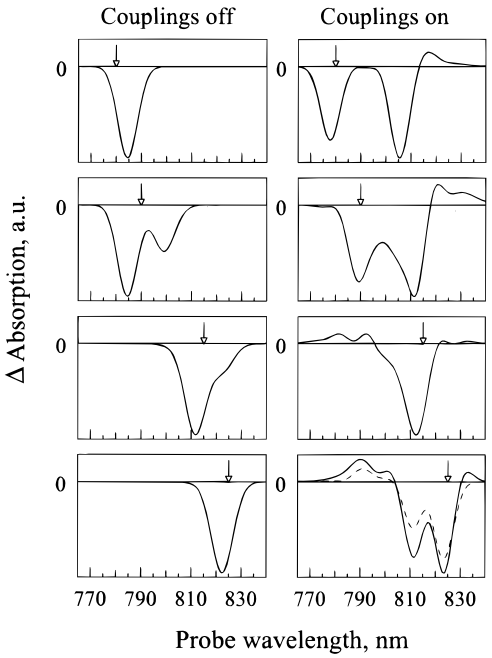

Figure 7. Prompt absorption difference spectra[44] simulated for *Pc. aestuarii* trimers using OKT diagonal energies. Excitation wavelengths (arrows) are 780, 790, 815, and 825 nm. Left-hand spectra were obtained with zero-resonance couplings H_{ij}; right-hand spectra were obtained with resonance couplings from ref 25. Sign convention is the same as in Figure 4.

expanded to first order in the $N(N-1)/2$ doubly excited basis functions $|\chi^{(2)}_{12}\rangle = |1*2*3...\rangle$, $|\chi^{(2)}_{13}\rangle = |1*23*...\rangle$, $|\chi^{(2)}_{23}\rangle = |12*3*...\rangle$, etc., describing excitations localized on pairs of pigments. The two-exciton levels $E^{(2)}_i$ are obtained by diagonalizing the Hamiltonian (eq 1) in this basis; the relevant matrix elements are

$$\langle\chi^{(2)}_{ij}|\hat{H}|\chi^{(2)}_{ij}\rangle = E_i + E_j$$

$$\langle\chi^{(2)}_{ij}|\hat{H}|\chi^{(2)}_{ik}\rangle = H_{jk}, \quad j \neq k$$

$$\langle\chi^{(2)}_{ij}|\hat{H}|\chi^{(2)}_{kl}\rangle = 0, \quad i \neq k, l; \quad j \neq k, l \qquad (5)$$

Here E_i, E_j are single-BChl diagonal energies, and the H_{jk} are identical to the ones in eq 3. At this level of approximation, evaluation of the two-exciton states thus requires no more information than the one-exciton states. Using these, the wavelengths and oscillator strengths of the ESA transitions can be directly determined, and the ΔA spectrum for FMO trimers prepared in a particular (set of) one-exciton level(s) can then be simulated, as has been described in detail in our earlier work.[44] Figure 7 shows prompt absorption difference spectra simulated for *Pc. aestuarii* trimers excited at 780, 790, 815, and 825 nm, using a 21-pigment model with no diagonal disorder (i.e., C_3 symmetry). These were obtained by dressing the stick spectra from the exciton calculations with 150 cm^{-1} fwhm symmetric Gaussian profiles. (Lu and Pearlstein[29] used 95−354 cm^{-1} fwhm Gaussians in their simulations of the steady-state PS and OKT spectra.) The right-hand spectra were computed from Pearstein's resonance couplings H_{ij}[28] and OKT diagonal energies;[29] the left-hand spectra were computed using all $H_{ij} = 0$, i.e., for an idealized FMO protein with noninteracting pigments. The Stokes shifts between PB and SE peaks were set equal to zero. (For FMO trimers from *P. aestuarii*, the low-temperature fluorescence band centroid emitted by the 827 nm exciton level appears at 828.3 nm;[21] this ∼20 cm^{-1} shift is considerably smaller than the separations between resolvable features in the steady-state absorption spectrum.) When the interactions are turned off, the effects on the prompt ΔA spectrum of tuning the laser from 780 to 825 nm are limited to red-shifting of a monomeric BChl *a* absorption difference spectrum across the set of single-site Q_y energies. The spectral evolution beomes more interesting when $H_{ij} \neq 0$: mixing occurs among the BChl Q_y states, and nominal PB/SE maxima now appear at wavelengths considerably removed from the laser wavelength, arising from "holes" in the one-exciton → two-exciton ESA spectrum that otherwise tends to cancel much of the PB/SE spectrum. Figure 8 compares ΔA spectra simulated[44] using the PS and OKT diagonal energies. Here, each curve is averaged over groups of three exciton levels and is labeled groups A−G in order of increasing energy (cf. Figure 2). The OKT ΔA spectrum for group A (the three lowest levels responsible for the 825 nm steady-state absorption band) shows bimodal features near 812 and 825 nm; the corresponding PS spectrum is dominated by a single broad PB/SE peak at ∼810 nm. The physical differences between these spectra are considerable. The OKT spectrum far more closely resembles the experimental spectrum at long times (e.g., 10 ps), when excitations will have become strongly concentrated in the group A levels at 19 K. Similar calculations using the Pearlstein interactions[28] and the Gülen diagonal energies (which assign the lowest site energy to pigment 6[34]) do not yield realistic ΔA spectra. (However, our experimental spectra and Pearlstein's resonance couplings are traceable to FMO proteins from *Cb. tepidum* and *Pc. aestuarii*, respectively. These comparisons may thus be colored by species variations, due to BChl conformational differences[13] in the two proteins.) In this sense, simulations of pump−probe ΔA spectra can serve as an additional criterion (besides absorption, LD, CD, and T−S absorption difference spectra) for exciton models of FMO electronic structure. Calculations of absorption difference spectra analogous to Figure 8, but limiting the exciton model to the seven BChl pigments in one subunit, yield spectra very similar to those from the 21-pigment model (not shown); these isotropic spectra are not strongly perturbed by the intersubunit couplings of ≤20 cm^{-1}.[28]

These simulations do not include the contribution of monomeric BChl *a* excited-state absorption (arising from transitions between the Q_y state to higher excited singlets). This monomeric BChl *a* ESA spectrum is several times broader than the inhomogeneous widths of the steady-state BChl *a* Q_y absorption band in polar solvents,[47] and its primary effect would be to add a positive baseline shift to the ΔA spectrum without significantly changing its structure. In simulations exploring the effects of exciton localization in ΔA spectra of LH2 antennas from purple bacteria,[48] incorporating monomeric ESA proved to be crucial, because localization effects in such antennas turn out to be relatively subtle. In our FMO simulations, PB/SE and one-exciton → two-exciton ESA (as modulated by the choice of diagonal energies) has far more leverage than monomeric ESA on the qualitative ΔA spectrum.

The simulated ΔA spectra in Figure 8 may be combined with kinetic models for relaxation between exciton level groups to generate three-dimensional surfaces of ΔA versus time and wavelength for comparison with the experimental surface (cf. Figure 4[44]). A kinetic model that yields a realistic surface (when combined with OKT simulations of single-level ΔA spectra) is shown in Figure 9. Here group F levels excited near 789 nm relax within 100 fs to group D levels, which account for the

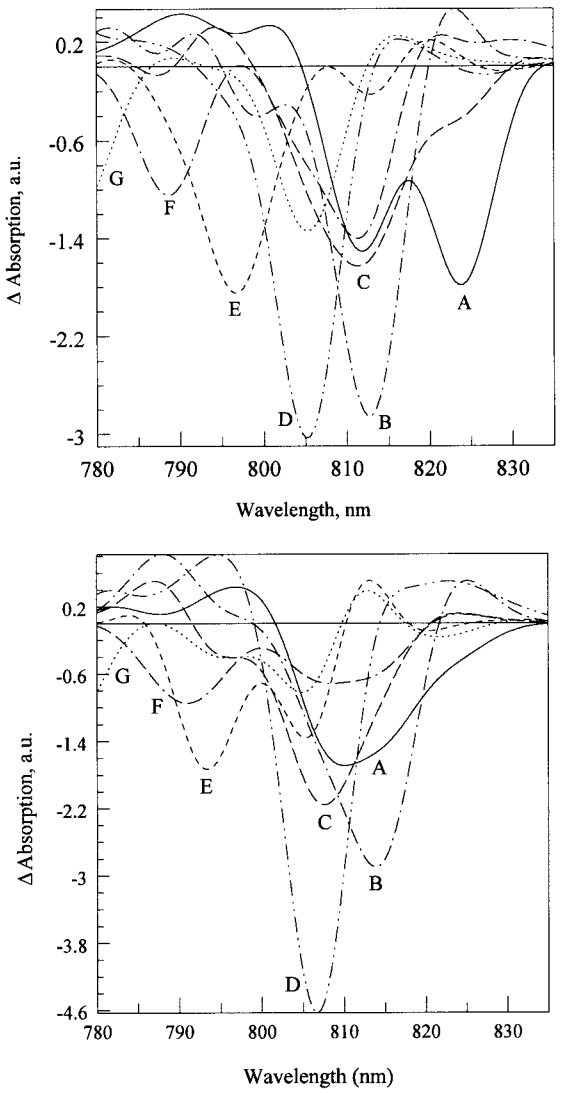

Figure 8. OKT (top) and PS (bottom) absorption difference spectra[44] simulated for *Pc. aestuarii* trimers excited in the level groups A, B, ..., G. Each spectrum is averaged over the three exciton states of the indicated group (cf. Figure 2).

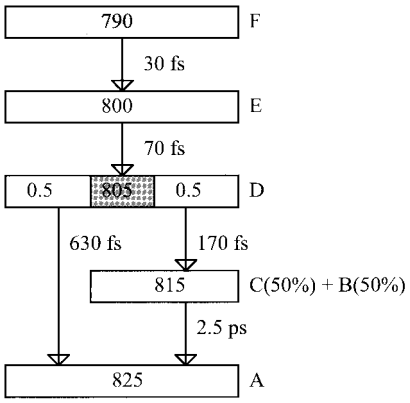

Figure 9. Kinetic model for exciton relaxation in FMO trimers, from OKT simulation of Δ*A* surface versus time and wavelength for *Pc. aestuarii* trimers excited at 789 nm. Labels A, B, ..., G indicate exciton level groups.[44]

steady-state absorption band near 805 nm (Figure 3). The group D levels then branch equally into group B and C levels clustered near 815 nm, with 170 and 630 fs kinetics, respectively. The group B/C levels cascade to group A with 2.5 ps kinetics. While this model probably depicts the processes terminating in level groups A−D fairly accurately (viz., Figure 6), the earliest events in Figure 9 may well be an artifact of the OKT simulations. The Δ*A* spectrum at 40 fs (Figure 4) shows, in addition to the strong PB/SE feature near the excitation wavelengths, a secondary PB/SE peak near 805 nm. The OKT simulation of the prompt Δ*A* spectrum predicts no such secondary peak (cf. Figure 7), and the model is thus forced to invoke rapid decay of group F into group D levels to account for this peak. Varying the porportions of group B and C levels populated by relaxation from group D has little influence on our simulations, since the former two groups have similar OKT spectra (Figure 8).

Finally, we note that the maximum PB/SE signals in the Δ*A* spectra of Figure 4 progressively decrease in the interval between 200 fs and 10 ps. (A coherent coupling artifact[49] contributes significantly to the very large "PB/SE" signal near 789 nm in the 40 fs Δ*A* spectrum, since this probe wavelength overlaps the laser excitation spectrum; it is not a true absorption difference signal.) This interesting behavior parallels a similar trend observed in time-resolved Δ*A* spectra of circular LH2 antennas from purple photosynthetic bacteria.[50] In a circular antenna with in-plane tangential BChl transition moments, more than half of the total ground → one-exciton oscillator strength is generally concentrated into a single exciton level when the excitation is localized to a segment of the circle. This level's dipole strength correlates with the number of coupled pigments (i.e., exciton size). Hence, the observed evolution toward smaller PB/SE signals in LH2 has been ascribed to dynamic exciton localization.[50] It appears unlikely to us that a similar cause underlies the spectral development in Figure 4. The FMO SE signal should decrease a priori (even in the absence of localization) when excitation migrates to levels responsible for the 825 nm steady-state absorption band, because the latter band's dipole strength is markedly lower than those of the 805 and 815 nm bands (cf. Figure 3). Moreover, most of the FMO laser-prepared states are already localized to two or three pigments at most (cf. Figure 11).

Optical Anisotropies and Localization

The foregoing isotropic absorption difference experiments have little bearing on the extent of exciton localization in FMO trimers, because 7- and 21-pigment exciton models (delocalized over one and three subunits of the trimer, respectively) predict similar Δ*A* spectra.[44] The question remains as to whether (a) the states are truly delocalized over all 21 pigments during the relaxation processes in Figure 9, (b) the laser-prepared states are essentially localized within one subunit of the trimer, or (c) the laser-prepared states are initially delocalized over the trimer, but evolve into more localized states because of dephasing by random protein motions, etc. Optical anisotropies are a potentially sensitive test for localization (Figure 10), because the exciton transition moments are markedly sensitive to extent of localization. This figure shows simulations[51] of two-color polarized Δ*A* spectra and prompt anisotropies as functions of the probe wavelength for *Pc. aestuarii* trimers excited at 815 or 825 nm (the longest-wavelength features in the steady-state absorption spectrum). The "monomer" and "trimer" anisotropies are computed using 7- and 21-pigment exciton models, respectively; they clearly give contrasting predictions. The experimental prompt anisotropies for *Cb. tepidum* trimers at 19 K are +0.35 and -0.30 in 815 → 815 and 825 → 815 two-color experiments, respectively. (These pump and probe wavelengths coincided with transitions to levels exhibiting relatively slow relaxation (Figure 9), and the laser spectra were chosen to avoid

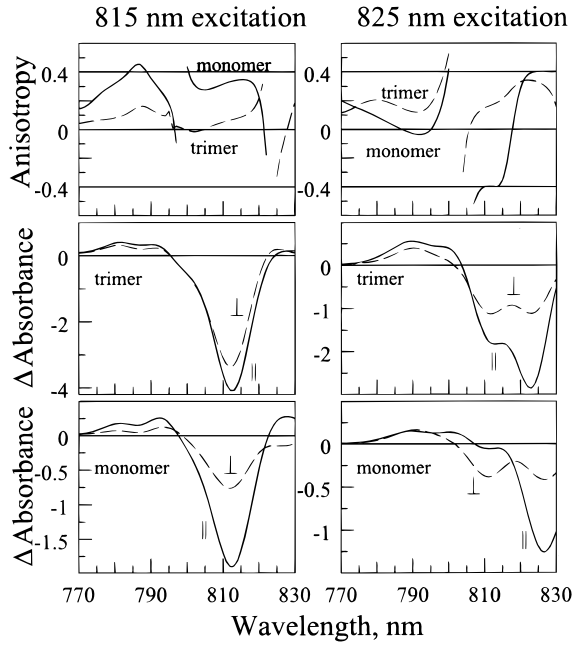

Figure 10. Two-color anisotropies (top) and polarized ΔA spectra (middle and bottom) simulated for *Pc. aestuarii* trimers excited with pump wavelengths 815 and 825 nm (left and right columns, respectively). Monomer and trimer curves denote 7- and 21-pigment models. Symbols || and ⊥ indicate parallel and perpendicular signals. Laser pulse spectra are 7 nm fwhm.[51]

coherences between the 825 and 815 nm level groups; see below.) These are far more similar to the OKT anisotropies predicted by the 7-pigment model than the 21-pigment model and thus suggest that typical laser-prepared states are essentially localized to one subunit of the trimer. This inference must be regarded with caution, because the realism of the OKT diagonal energies is not well established and because the anisotropies and simulations are derived from *Cb. tepidum* and *Pc. aestuarii*, respectively. The conclusion is nevertheless reasonable, because the ~70 cm^{-1} inhomogeneous broadening for the lowest exciton levels in *Cb. tepidum* is several times larger than the ~20 cm^{-1} resonance coupling between BChls belonging to different subunits. While such inhomogeneous broadening is considerably smaller than that found in the purple bacterial LH1 and LH2 antennas, the underlying static disorder has considerably more leverage than in LH1/LH2 (where the couplings between adjacent BChls in these circular antennas are in the hundreds of cm^{-1} [50,52]). As a result, most of the FMO exciton states in a laser-excited ensemble may be regarded as confined within a subunit.

In fact, the OKT model predicts that the laser-prepared states are considerably more localized than this, owing to large diagonal energy dispersion among nonequivalent BChls (Figure 2). Figure 11 shows excitation densities on each of the pigments in the lowest four exciton levels in the seven-pigment model. With the exception of the 812 nm state, the laser-prepared states are already localized to two or three pigments at most. Exciton localization has currently been a major issue in LH2 antennas,[50,52] which (in the case of *Rps. acidophila*) contain two sets of nine equivalent BChls in a circular arrangement. Here the idealized 18-pigment exciton domain for a perfect C_9-symmetric protein is reduced to two to four BChls by a combination of static and dynamic disorder at room temperature.[50,52] If the OKT model is correct, localization is a nonissue in the FMO proteins, where static disorder and diagonal energy dispersion typically limit excitations to two or three pigments even at 19 K (Figure 11).

Coherent Oscillations and Quantum Beating

The one-color optical anisotropies of FMO trimers from *Cb. tepidum* show strong oscillations at 19 K[53] when the pump−probe laser spectrum simultaneously overlaps both the 815 and 825 nm bands of the steady-state spectrum (Figure 12). When the laser spectrum overlaps only one of these bands, the amplitude of the oscillations is considerably diminished. The oscillations in the polarized absorption difference signals $\Delta A_{||}(t)$ and $\Delta A_{\perp}(t)$ are out-of-phase, and they nearly cancel in the isotropic signal $\Delta A_{||}(t) + 2\Delta A_{\perp}(t)$ (upper right inset in Figure 12). Their 220 fs period matches the 150 cm^{-1} energy separation between the 815 and 825 nm level groups. Hence,

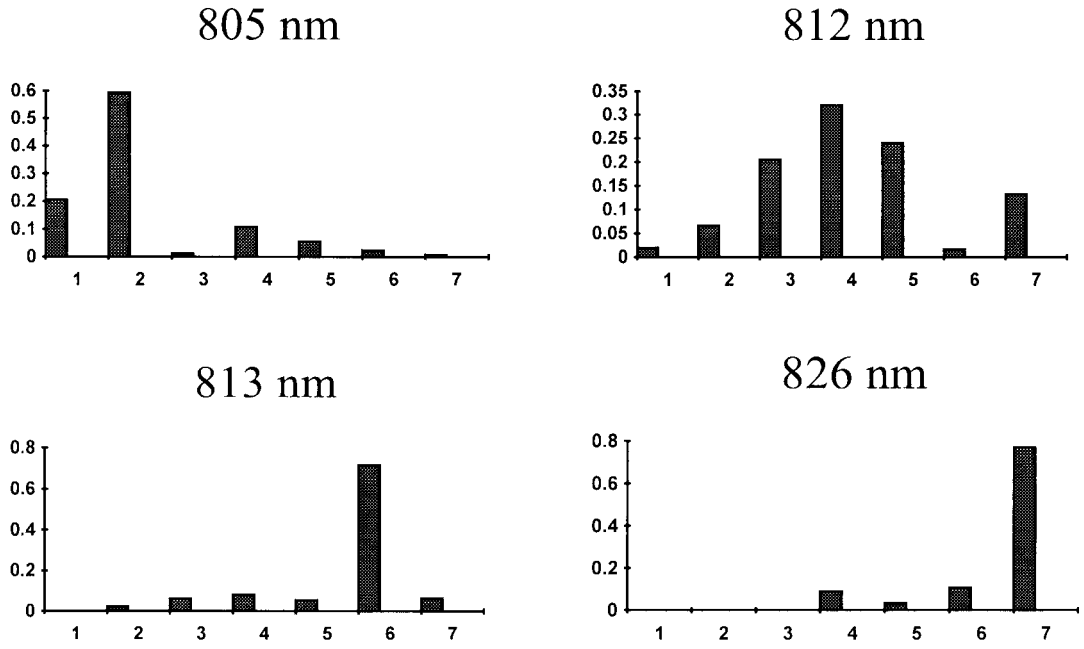

Figure 11. Excitation densities c_{ij}^2 on BChls 1−7, evaluated from an OKT simulation of one-exciton states $|\psi_i^{(1)}\rangle = \sum_j c_{ij}|\chi_j^{(1)}\rangle$ in a seven-pigment model.

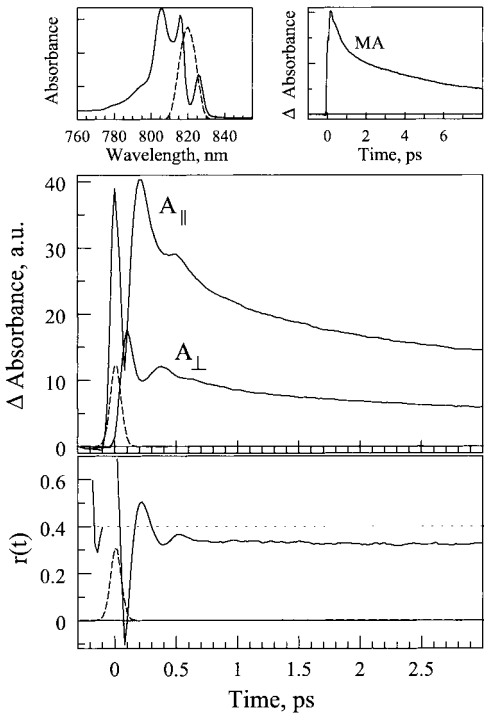

Figure 12. Polarized absorption difference signals $\Delta A_{\parallel}(t)$, $\Delta A_{\perp}(t)$ and the anisotropy $r(t)$ for *Cb. tepidum* trimers excited at 820 nm.[53] Laser spectrum, which straddles the 815 and 825 nm absorption bands, is shown by dashed curve at upper right inset. Signals are dominated by PB/SE throughout.

they are not vibrational coherences,[54,55] but appear to be quantum beats that stem from coherent excitation of levels within the respective groups. In the simplest version of this picture, the broad laser spectrum in Figure 12 prepares a coherent superimposition[56]

$$|\psi(t)\rangle = a_1|1\rangle e^{-iE_1t/\hbar} + a_2|2\rangle e^{-iE_2t/\hbar} \qquad (6)$$

of exciton states $|1\rangle$ and $|2\rangle$ belonging to the 825 and 815 nm sets of levels (groups A and B,C, respectively). The resulting time-dependent anisotropy (for early times prior to relaxation between exciton components) is then equal to[53]

$$r(t) = 0.4\frac{2I_{r1}I_{u1} + 2I_{r2}I_{u2} + \frac{1}{2}(\gamma^2+3)\sqrt{I_{r1}I_{r2}I_{u1}I_{u2}}\cos(\Delta Et/\hbar)}{2I_{r1}I_{u1} + 2I_{r2}I_{u2} + \gamma^2\sqrt{I_{r1}I_{r2}I_{u1}I_{u2}}\cos(\Delta Et/\hbar)} \qquad (7)$$

when the absorption difference signal is dominated by PB/SE. (This result differs from the fluorescence anisotropy,[57,58] in which the nonoscillating PB contributions are absent.) Here γ is the scalar product of transition moments for the exciton bands $|1\rangle$ and $|2\rangle$; ΔE is their energy separation; and I_{u1}, I_{r1} are the laser pump and probe intensities, multiplied by the optical densities of the one-exciton absorption band for state $|1\rangle$ at the respective wavelengths (and similarly for I_{r2}, I_{u2}). If the two transition moments are essentially perpendicular (i.e., $\gamma \sim 0$; the OKT simulations predict that the 815 and 825 nm level groups are dominated by mutually perpendicular transitions[53]), the oscillations in $r(t)$ exhibit maximum amplitude. The isotropic signal (which is the denominator in eq 7) concomitantly shows no oscillatory term; this resembles the situation in Figure 12. Under these circumstances, $r(t)$ is expected to swing between 0.10 and 0.30 if the two exciton bands are equally excited ($I_{r1} = I_{u1} = I_{r2} = I_{u2}$). The observed oscillations are considerably larger than this ($r(t)$ peaks above 0.4 at times well beyond the instrument function in Figure 12), but it is easily shown that the presence of ESA transitions to two-exciton levels can account for this.[53] The oscillations are damped with 140−180 fs lifetimes. Such rapid damping (whose time scale is similar to the oscillation period itself) arises from superimposing quantum beats between levels (separated by $\sim$150 cm^{-1}) that are broadened by $\sim$70 cm^{-1} diagonal energy disorder. The damping time does not reflect exciton coherence decay; accumulated photon echo experiments on *Pc. aestuarii* trimers[59] suggest that this process requires several hundred picoseconds in the lowest exciton levels at low temperatures.

Future Prospects

Femtosecond pump−probe spectroscopy can clearly reveal a wealth of detailed, *phenomenological* information about relaxation kinetics and excitation localization in spectrally heterogeneous photosynthetic antennas. A major impediment to molecular-level interpretations of such experiments is the absence of a reliable theory for protein site effects on pigment properties such as Q_y energies and resonance interactions. Such a theory would greatly facilitate the assignment of exciton level parentages in the FMO protein and would point the way to sifting out the dominant mechanisms for interexciton relaxation (nonadiabatic couplings $\partial V_{ij}/\partial Q$ arising from influence of nuclear coordinates on resonance couplings,[21] dynamic disorder arising from fluctuations in diagonal energies E_i,[60] etc.). Similar problems exist in other antennas with multiple inequivalent pigments (14 sites in the LHC-II antenna protein of green plant photosystem II,[9] $\sim$100 in the photosystem I core antenna[10]). In short, the next significant advances in our understanding of the FMO protein appear more likely to emerge from theory (or mutagenesis) than from ultrafast absorption difference spectroscopy.

Acknowledgment. We acknowledge the people who assisted in the earlier FMO experiments and exciton modeling: Timothy Causgrove, Shumei Yang, Paul Lyle, Herbert van Amerongen, and Su Lin. We thank Roger Fenna, Robert Blankenship, and Wenli Zhou for providing FMO protein preparations. The Ames Laboratory is operated for the U.S. Department of Energy by Iowa State University under Contract No. W-7405-Eng-82. This work was supported by the Division of Chemical Sciences, Office of Basic Energy Sciences.

References and Notes

(1) Blankenship, R. E.; Olson, J. M.; Miller, M. In *Anoxygenic Photosynthetic Bacteria*; Blankenship, R. E., Madigan, M. T., Bauer, C. E., Eds.; Kluwer: Dordrecht, 1995; pp 399−435.

(2) Staehelin, L. A.; Golecki, J. R.; Fuller, R. C.; Drews, G. *Arch. Microbiol.* **1978**, *119*, 269.

(3) Olson, J. M. *Biochim. Biophys. Acta* **1980**, *594*, 33.

(4) Deisenhofer, J.; Epp, O.; Miki, R.; Huber, R.; Michel, H. *Nature* **1985**, *318*, 618.

(5) Fenna, R. E.; Matthews, B. W.; Olson, J. M.; Shaw, E. K. *J. Mol. Biol.* **1974**, *84*, 231.

(6) Matthews, B. W.; Fenna, R. E.; Bolognesi, M. C.; Schmid, M. F.; Olson, J. M. *J. Mol. Biol.* **1979**, *131*, 259.

(7) Matthews, B. W.; Fenna. R. E. *Acc. Chem. Res.* **1980**, *13*, 309.

(8) Olson, J. M.; Romano, C. A. *Biochim. Biophys. Acta* **1962**, *59*, 726.

(9) Kühlbrandt, W.; Wang, D. N. *Nature* **1991**, *350*, 130.

(10) Krauss, N.; Hinrichs, W.; Witt, I.; Fromme, P.; Pritzkow, W.; Dauter, Z.; Betzel, C.; Wilson, K. S.; Witt, H. T.; Saenger, W. *Nature* **1993**, *361*, 326.

(11) McDermott, G. S.; Prince, M.; Freer, A. A.; Hawthornthwaite-Lawless, A. M.; Papiz, M. Z.; Cogdell, R. J.; Isaacs, N. W. *Nature* **1995**, *374*, 517.

(12) Schirmer, T.; Bode, W.; Huber, R.; Sidler, W.; Zuber, H. *J. Mol. Biol.* **1985**, *184*, 257.
(13) Li, Y.-F.; Zhou, W.; Blankenship, R. E.; Allen, J. P. *J. Mol. Biol.* **1997**, *271*, 456.
(14) Daurat-Larroque, S. T.; Brew, K.; Fenna, R. E. *J. Biol. Chem.* **1986**, *261*, 3607.
(15) Dracheva, S.; Williams, J. C.; Blankenship, R. E. In *Research in Photosynthesis*; Murata, N., Ed., Kluwer: Dordrecht, 1992; Vol. I, pp 53−56.
(16) Tronrud, D. E.; Schmid, M. F.; Matthews, B. W. *J. Mol. Biol.* **1986**, *188*, 443. Tronrud, D. E.; Matthews, B. W. In *The Photosynthetic Reaction Center*; Norris, J., Deisenhofer, H., Eds.; Academic Press: San Diego, 1993; Vol. I, pp 13−21.
(17) Sundström, V.; van Grondelle, R. In *Anoxygenic Photosynthetic Bacteria*; Blankenship, R. E., Madigan, M. T., Bauer, C. E., Eds.; Kluwer: Dordrecht, 1995; pp 349−372.
(18) Debreczeny, M. P.; Sauer, K. *J. Phys. Chem.* **1995**, *99*, 8412−8419. Debreczeny, M. P.; Sauer, K., *J. Phys. Chem.* **1995**, *99*, 8420−8431, and references therein.
(19) Philipson, K. D.; Sauer, K. *Biochemistry* **1972**, *11*, 1880.
(20) Olson, J. M.; Ke, B.; Thompson, K. H. *Biochim. Biophys. Acta* **1976**, *430*, 524.
(21) Johnson, S. G.; Small, G. J. *J. Phys. Chem.* **1991**, *95*, 471.
(22) Reddy, N. R. S.; Jankowiak, R.; Small, G. J. *J. Phys. Chem.* **1995**, *99*, 16168.
(23) Van Mourik, F.; Verwijst, R. R.; Mulder, J. M.; van Grondelle, R. *J. Phys. Chem.* **1995**, *98*, 10307.
(24) Olson, J. M. In *The Chlorophylls*; Vernon, L. P., Seely, G. R., Eds.; Academic Press: New York, 1966; pp 413−425.
(25) Whitten, W. B.; Pearlstein, R. M.; Phares, E. F.; Geacintov, N. E. *Biochim. Biophys. Acta* **1978**, *503*, 491.
(26) Förster, T. *Ann. Phys. (Leipzig)* **1948**, *2*, 55.
(27) Pearlstein, R. M.; Hemenger, R. P. *Proc. Natl. Acad. Sci. U.S.A.* **1978**, *75*, 4920.
(28) Pearlstein, R. M. *Photosynth. Res.* **1992**, *31*, 213.
(29) Lu, X.; Pearlstein, R. M. *Photochem. Photobiol.* **1993**, *57*, 86.
(30) Chang, J. C. *J. Chem. Phys.* **1977**, *67*, 3901.
(31) Weiss, C. *J. Mol. Spectrosc.* **1972**, *44*, 37.
(32) Gottfried, D. S.; Stocker, J. W.; Boxer, S. G. *Biochim. Biophys. Acta* **1991**, *1059*, 63. Beekman, L. M. P.; Steffen, M.; van Stokkum, I. H. M.; Olsen, J. D.; Hunter, C. N.; Boxer, S. G.; van Grondelle, R. *J. Phys. Chem. B* **1997**, *101*, 7284.
(33) Gudowska-Nowak, E.; Newton, M. D.; Fajer, J. *J. Phys. Chem.* **1990**, *94*, 5795.
(34) Gülen, D. *J. Phys. Chem.* **1996**, *100*, 17683.
(35) Louwe, R. J. W.; Vrieze, J.; Hoff, A. J.; Aartsma, T. J. *J. Phys. Chem.*, in press.
(36) Alden, R. G.; Johnson, E.; Nagarajan, V.; Parson, W. W.; Law, C. J.; Cogdell, R. G. *J. Phys. Chem. B* **1997**, *101*, 4667.
(37) Buck, D. R.; Savikhin, S.; Struve, W. S. *J. Phys. Chem. B* **1997**, *101*, 8395.
(38) Savikhin, S.; Zhou, W.; Blankenship, R. E.; Struve, W. S. *Biophys. J.* **1994**, *66*, 110.
(39) Savikhin, S.; Struve, W. S. *Biochemistry* **1994**, *33*, 11200.
(40) Causgrove, T. P.; Yang, S.; Struve, W. S. *J. Phys. Chem.* **1988**, *92*, 6790.
(41) Lyle, P. A.; Struve, W. S. *J. Phys. Chem.* **1990**, *94*, 7338.
(42) Knox, R.S. In *Bioenergetics of Photosynthesis*; Govindjee, Ed.; Academic Press: New York, 1975; pp 183−221.
(43) Lyle, P. A.; Struve, W. S. *Photochem. Photobiol.* **1991**, *53*, 359.
(44) Buck, D. R.; Savikhin, S.; Struve, W. S. *Biophys. J.* **1997**, *72*, 24.
(45) Freiberg, A.; Lin, S.; Zhou, W.; Blankenship, R. E. In *Ultrafast Processes in Spectroscopy*; Svelto, O., De Silvestri, S., Denardo, G., Eds.; Plenum Press: New York, 1996.
(46) Vulto, S.; Streltsov, A. M.; Aartsma, T. J. *J. Phys. Chem. B* **1997**, *101*, 4845.
(47) Becker, M.; Nagarajan, V.; Parson, W. W. *J. Am. Chem. Soc.* **1991**, *113*, 6840.
(48) Pullerits, T.; Chachisvilis, M.; Sundström, V. *J. Phys. Chem.* **1996**, *100*, 10787.
(49) Chachisvilis, M.; Sundström, V. *J. Chem. Phys.* **1996**, *104*, 5734.
(50) Kennis, J. T. M; Streltsov, A. M.; Permentier, H.; Aartsma, T. J. *J. Phys. Chem. B* **1997**, *101*, 8369. Nagarajan, V. N.; Alden, R. G.; Williams, J. C.; Parson, W. W. *Proc. Natl. Acad. Sci. U.S.A.* **1996**, *93*, 13774.
(51) Savikhin, S.; Buck, D. R.; Struve, W. S. *Biophys. J.* **1997**, *73*, 2090.
(52) Pullerits, T.; Sundström, V. *Acc. Chem. Res.* **1996**, *29*, 381. Chachisvilis, M.; Kühn, O.; Pullerits, T.; Sundström, V. *J. Phys. Chem. B* **1997**, *101*, 7275. Monshouwer, R.; Abrahamsson, M.; van Mourik, F.; van Grondelle, R. *J. Phys. Chem. B* **1997**, *101*, 7241.
(53) Savikhin, S.; Buck, D. R.; Struve, W. S. *Chem. Phys.* **1997**, *223*, 303.
(54) Chachisvilis, M.; Pullerits, T.; Jones, M. R.; Hunter, C. N.; Sundström, V. In *Ultrafast Phenomena IX: Proceedings of the 9th International Conference*; Barbara, P. F., Knox, W. H., Mourou, G. A., Zewail, A. H., Eds.; Dana Point, CA, May 2−6, 1994; Springer-Verlag: Berlin, 1994; pp 435−436.
(55) Savikhin, S.; Zhu, Y.; Lin, S.; Blankenship, R. E.; Struve, W. S. *J. Phys. Chem.* **1994**, *98*, 10322.
(56) Avouris, P.; Gelbart, W. M.; El-Sayed, M. A. *Chem. Rev.* **1977**, *77*, 793.
(57) Knox, R. S.; Gülen, D. *Photochem. Photobiol.* **1993**, *57*, 40.
(58) Wynne, K.; Hochstrasser, R. M. *Chem. Phys.* **1993**, *171*, 179.
(59) Loewe, R. J. W.; Aartsma, T. J. *J. Lumin.* **1994**, *58*, 154.
(60) Van Grondelle, R.; Dekker, J. P.; Gillbro, T.; Sundström, V. *Biochim. Biophys. Acta* **1994**, *1187*, 1.